Applied Chemical Engineering (2024) Volume 7 Issue 2
doi: 10.59429/ace.v7i2.2064

ORIGINAL RESEARCH ARTICLE

Behavior of enzymatic membranes under pressure: Effect of enzyme location

Yilmaz Yurekli[1,2,*], Sadika Guedidi[3] , Sacide Alsoy Altinkaya[2], André Deratani[3], Christophe Innocent[3]

[1] *Bioengineering Department, Manisa Celal Bayar University, Manisa 45140, Turkey*

[2] *Department of Chemical Engineering, Izmir Institute of Technology, Gulbahce Kampusu, Urla 35430, Turkey*

[3] *European Membrane Institute, Montpellier 2 University (ENSCM, UM2, CNRS), F-34095 Montpellier Cedex 5, France*

* **Corresponding author:** Yilmaz Yurekli, yilmazyurekli@gmail.com

ABSTRACT

Enzyme immobilized membranes combine catalysis and separation functions. Their application in large-scale continuous processes requires knowing the behavior under pressure. Also, the effects of enzyme location on the mass transfer limitation, membranes' stability, and filtration performance should be investigated. In this study, urease (URE) and trypsin (TRY) enzymes were physically immobilized in/on the surface of a polyacrylonitrile (AN69) membrane through layer-by-layer (LbL) self-assembly method using polyethylenemine (PEI) and sodium-alginate (ALG) as cationic and anionic polyelectrolytes respectively. URE, located on the membrane's surface, degraded urea in a reaction-controlled regime, and its immobilization did not significantly change the hydraulic permeability. On the other hand, the TRY enzyme attached to the membrane's pores reduced the permeability and degraded the BAPNA in a diffusion-controlled region. In TRY immobilized membranes, the conversion increased linearly with the transmembrane pressure, while in URE immobilized ones, conversion was maximum at 1 bar. Sandwiching the enzymes between two polyelectrolytes resulted in the highest catalytic activities. This configuration maintained most of the URE activity in the long-term filtration, but it did not help prevent TRY's activity loss.

Keywords: enzymatic membrane; LbL self assembly; mass transfer resistance; long term stability; trypsin; urease

ARTICLE INFO

Received: 9 June 2023
Accepted: 12 September 2023
Available online: 3 April 2024

1. Introduction

The unique porous structure and physicochemical features of membranes make them ideal for enzymatic reaction and simultaneous separation. Their outstanding features, including high selectivity, stability, and productivity, can be reached by precise tuning of design parameters consisting of enzyme loading and enzyme locations. Enzymes are either immobilized on the surface or entrapped in the pores of the membrane. The enzyme location significantly influences the catalytic performance of the membrane. Due to diffusional limitations, enzymes in the membrane's pores lower the flux and encounter lower substrate concentrations than the enzymes located on the membrane surface; hence their activity is lower[1]. However, this case, to some extent, may be helpful to specific reactions at which substrate has a strong inhibition effect[1,2]. Although enzymes immobilized on the membrane surface enable high conversion, back-diffusion of products may adversely affect the reactor performance through product inhibition. Generally, back diffusion can be neglected at high transmembrane pressure (TMP) or fluxes. However, in this

case, the rate at which fouling occurs on the surface may increase, or the rate of substrate conversion may decrease (lower productivity). Furthermore, a higher pressure may lead to the detachment of the enzyme molecules from the membrane surface due to the increased hydraulic shear force. The enzyme location also influences the long-term stability of the membrane. The pore size of a porous membrane relative to the size of an enzyme has a strong effect on the activity. While pore size ranging between 2–50 nm enables superior conformational stability to the immobilized enzyme without restricting enzyme access, beyond this range, the enzyme encounters either a physical restriction in accessing to the pores or coalesce in the pores due to protein-protein interactions[3]. If the enzyme is on the surface, the TMP becomes an essential factor in its conformational stability. The choice for the enzyme location is then determined by the decision between the long-term stability and the impact of mass transfer resistance on reaction rate. This study investigates the effect of enzyme location on the catalytic activity (conversion), long-term stability (reusability), and the rate-limiting step under dynamic conditions.

The immobilization method determines the bonding strength between enzyme molecules and functional groups of the membrane and enzyme conformation stability. While the physical adsorption method cannot prevent the enzyme's leaching, the covalent bonding method causes the enzyme's partial inactivation. The layer-by-layer (LbL) self-assembly of polyelectrolytes meets the above requirements satisfactorily, providing a one-step, defect-free, ultrathin and stable deposition of enzymes. The method can be applied on any curved or flat, negatively or positively charged surfaces. Besides, it is an environmentally benign process involving an aqueous solution as the media at moderate temperatures. Many studies utilized LBL assembly to develop, for example, biosensors, biocatalysts[4,5], and nanofiltration membranes[6] with enzyme immobilization. These studies focus on optimizing biocatalytic activity under static conditions. However, in industry, enzymatic membrane reactors are mainly operated under pressure-driven continuous flow mode; hence, the membranes' activity and stability under dynamic conditions should be elaborated. This knowledge is necessary for an accurate design or optimization of operating conditions of the enzymatic reactors. Only a few studies investigated the behavior of LBL-enzyme assembly under dynamic conditions[7–9]. In these studies, the enzymes were immobilized in the membrane's pores, and the effects of permeate flux[7–9] and the pore size[9] on the catalytic activity were investigated. Although kinetic parameters were determined under dynamic conditions; the enzyme's long-term stabilities were evaluated with the static experiments[7,8].

In our previous study, the LbL technique was employed for the immobilization of urease (URE) and trypsin (TRY) on the surface or within the pores of the AN69 ultrafiltration membrane using PEI and ALG as cationic and anionic polyelectrolytes[10]. We have found that the long-term enzyme stability in a batch mode can significantly improve when a thin polyelectrolyte layer covers the enzyme on the outermost layer. In this study, we aimed to test the performance of the AN69 based membranes created with different LbL architectures using the same polyelectrolytes and enzymes under dynamic conditions since most enzymatic membrane bioreactors are operated continuously. We particularly focused on investigating the effect of enzyme location and the different LbL architectures on enzyme activity, stability, and mass transfer limitations.

2. Materials and methods

2.1. Materials

Commercially available PAN-based flat sheet membranes, prepared by the copolymerization of acrylonitrile and sodium methallyl sulfonate monomers, were supplied by Gambro, Hospal, France, and used as support material. The commercial membrane, denoted as AN69, is negatively charged due to the ionized sulfonate groups' presence in its backbone and has a molecular weight cut-off of 30 kDa. The producer modifies the surface of the AN69 membrane with PEI adsorption and denotes this membrane as AN69-PEI. The wet thickness, pore radius, and porosity of the AN69 membrane are 25 mm, 20 ± 6 nm, and 0.8,

respectively[10–12]. Sigma supplied polyethyleneimine (PEI), sodium alginate (ALG) Jack bean urease type III (EC 3.5.1.5 and U1500-20KU, 40 U/mg solid), Trypsin (23.8 kDa) from bovine pancreas type XII-S (EC 3.4.21.4 and ≥ 9000 BAEE U/mg solid), N-benzoyldl- arginine-p-nitroanilide (BAPNA) and Bradford reagent (B 6916). Urea, trizma hydrochloride, phosphate buffer, sodium nitroprusside dihydrate, and acetic acid were purchased from Fluka. Phenol (Rectabur > 99%), sodium hydroxide anhydrous pellets (Carlo Erba > 97%), sodium hypochlorite (Riedel, 6%–14% Cl active), were obtained from different companies. All aqueous solutions were prepared with Milli-Q water (> 18 MWcm). The trypsin purity was determined to be 90% using chromatography on a Superose 12 column and that of urease to be 3.47% using the Bradford method[13]. According to the latter method, 1 mL of enzyme solution was mixed with 1 mL of Bradford reagent. Following 10 min of incubation, the concentration was determined at 595 nm using a UV/VIS spectrophotometer.

2.2. Methods

2.2.1. Fabrication of TRY and URE ımmobilized AN69-PEI membranes

The protocol for TRY and URE's immobilization on the AN69-PEI membranes has been described in detail in our previous study[10]. Briefly, the reactive TRY membranes were fabricated by successive immersion of (AN69-PEI) membrane in ALG and TRY giving the (AN69-PEI-ALG-TRY) membrane and in ALG, TRY and ALG giving the (AN69-PEI-ALG-TRY-ALG) membrane. Similarly, reactive URE membranes (AN69-PEI-URE and AN69-PEI-URE-PEI) were prepared using the same approach. Each stage of adsorption was followed by rinsing the membrane in the corresponding buffer solution to remove excess polyelectrolyte.

2.2.2. Filtration studies

The membrane's catalytic performances under dynamic conditions were characterized using a dead-end stirred cell filtration system (Model 8010, Millipore Corp, Bedford, MA, internal volume: 10 mL, active surface area: 4.1 cm^2). The feed side pressure was maintained by nitrogen, and the feed solution was continuously stirred (300 rpm) to avoid concentration polarization. Filtrate samples were collected at several transmembrane pressures and measured using an analytical balance (Sartorius BP221S with an accuracy of 0.1 mg) (**Figure 1**). In all experiments, the temperature was maintained at 23 ± 2 °C. First, the AN69-PEI membrane was placed into the cell and compacted with water twice up to 2 bars by a gradual increase in pressure necessary to keep the membrane morphology stable. After reaching a steady-state, filtration of 22 mM phosphate buffer at pH 7 and 100 mM Trizma buffer at pH 8 through URE and TRY immobilized membranes was carried out at three different levels of transmembrane pressures (0.5 bar, 1.0 bar, and 1.5 bar). Finally, urea (0.5–50 mM) and BAPNA (0.05–2 mM) solutions were filtered for 10 minutes at each transmembrane pressure, and samples were taken from permeate and retentate streams. TRY hydrolyzes BAPNA into N-benzoyl arginine and the yellow-colored p-nitroaniline (p-NA) while URE catalyzes urea's hydrolysis into ammonium and carbon dioxide. The concentrations of BAPNA and p-NA (CBAPNA and Cp-NA) in the samples were determined spectrophotometrically by reading their absorbances at 315 and 410 nm, respectively. Ammonia concentration was determined by mixing 40 µL of the sample with 20 mL of 10% acetic acid solution. 20 mL from this mixture was poured into a tube which consisted of 5 mL of reagent-A (5 g of phenol with 25 mg of sodium nitroprusside diluted to 500 mL with water). After shaking gently, 5 mL of reagent-B (2.5 g of sodium hydroxide and 4.2 mL of sodium hypochlorite diluted to 500 mL with water) was added. The mixture was then incubated at 37 °C for 20 min. The color change during incubation related to the liberated ammonium concentration (C1) was detected at a wavelength of 625 nm using a Perkin Elmer UV/VIS Spectrophotometer. The total amount of urea in the samples was determined through enzymatic decomposition. For this purpose, 60 µL of urea solution was reacted with 10 µL of URE (0.347 mg urease/mL solution was used in 22 mM buffer at pH 7) at 37 °C for 60 min. The reaction was stopped with 35 µL of 10% acetic acid. 60 min was enough to convert all the urea to ammonia, and its concentration was determined following the same procedure given above (C2). The unreacted urea concentration was calculated by subtracting C1 from

C2 and then dividing it to 2. The following expression calculated the specific activities, V_i, (mmol/min.mg) for both TRY and URE immobilized membranes,

$$V_i = \frac{A \times V}{t \times \varepsilon \times l \times m} \quad (1)$$

where, A represents absorbance value of the product, V is the volume of the sample (mL), t, e, l, and m stands for the filtration time (min), extinction coefficient ($M^{-1}cm^{-1}$), optical path length (cm), and amount of immobilized enzyme, respectively. The membranes' surface densities given in **Table 1** were used to calculate the amount of the immobilized enzyme for a given surface area of the membrane.

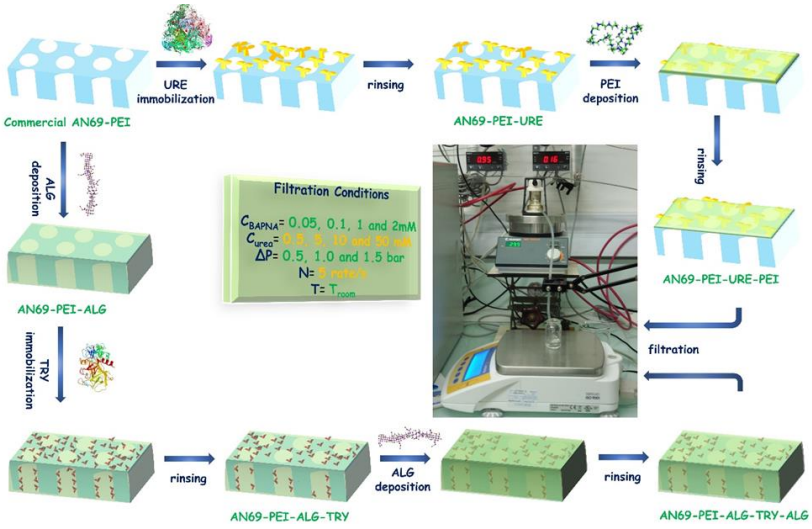

Figure 1. Experimental protocol for the filtration of urea and BAPNA through URE and TRY immobilized membranes.

Table 1. Amount of enzymes immobilized on/in the membranes[10].

Membranes	Γ (mg cm^{-2})
AN69-TRY	0.21
AN69-PEI-ALG	0.22
AN69-PEI-ALG-TRY-ALG	0.15
AN69-PEI-URE	0.01
AN69-PEI-URE-PEI	0.01

The filtration data were used to calculate the solution flux, J_v (L/m^2 h) by dividing the slope of the volumetric flowrate, V_p (L/h), through the membrane to the effective membrane area, A (m^2),

$$J_v = \frac{V_p}{A} \quad (2)$$

The hydraulic permeability, L_p (L/m^2 h bar), through the membrane was determined from the slope of the solution flux's plot as a function of transmembrane pressure.

$$L_p = \frac{J_v}{\Delta P} \quad (3)$$

The viscosity correction term in Equation (3) was neglected due to a slight temperature variation during the experiments.

2.2.3. Determination of kinetic parameters

The kinetics of immobilized enzymes were determined by measuring the products' concentration in the retentate and permeate solution with increased substrate concentrations in the feed solution. The data were then evaluated with the Michaelis-Menten equation, and the kinetic parameters, V_{max} and K_m, were obtained

from the non-linear regression analysis based on the Michaelis-Menten expression.

$$V_i = \frac{V_{\max}[S]}{K_m + [S]} \tag{4}$$

where, V_{max} (kmol/m^2 s) is the maximum reaction rate possible if every enzyme molecule is saturated with substrate, and K_m (kmol/m^3) defines the substrate concentration at which the observed reaction rate is half of V_{max}.

2.2.4. Determination of retained activity at the end of the filtration

Before filtration, a small piece of enzyme immobilized membrane was immersed into substrate solution. The product's concentration liberated from the catalytic reaction was determined according to the protocol described in section 2.2.2. This measurement was repeated at the end of the filtration with the membrane used in the experiment. The percentage of retaining activity was calculated by dividing the observed activity after filtration by the value obtained before filtration. The details for the measurement of TRY and URE's immobilized activities can be found in our previous work[10].

2.2.5. Effects of mass transfer resistance on the ımmobilized enzyme kinetics

Under dynamic conditions, mass transfer resistances present during substrate filtration are shown in **Figure 2**. Previously, we have shown that URE is immobilized on the surface, whereas TRY inside the membrane's pores. In the case of URE immobilized membrane, urea first diffuses to the enzyme surface, and then reaction occurs at the surface. The relative importance of the mass transfer compared to the enzymatic degradation of urea can be determined by a dimensionless number called Damköhler. The Damköhler number can be interpreted as the maximum reaction rate ratio to the maximum mass transfer rate.

$$D_a = \frac{V_{\max}}{K_0 S_0} \tag{5}$$

where, S_0 (kmol/m^3) is the initial substrate concentration. If $D_a \leq 1$, the maximum mass-transfer rate is much larger than the maximum rate of reaction, and the process is said to be in the reaction-limited regime. On the other hand, when the mass-transfer resistance is large, mass transfer is the limiting process, and $D_a \geq 1$ (m/s) in Equation (5) corresponds to the overall mass transfer coefficient. It is obtained from the sum of all resistances shown in **Figure 2**.

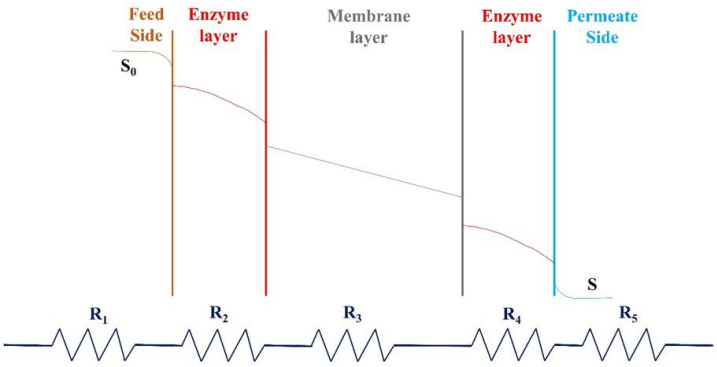

Figure 2. The variation of substrate concentration through an enzymatic membrane under dynamic condition.

$$R_T = R_1 + R_2 + R_3 + R_4 + R_5 = \frac{1}{K_0} = \frac{1}{k_s} + \frac{L_{\text{enz}}}{D_e} + \frac{L_{\text{mem}}}{D_m} + \frac{L_{\text{enz}}}{D_e} + \frac{1}{k_p} \tag{6}$$

In Equation (6), L_{mem} (m), L_{enz} (m), D_m (m^2/s), and D_e (m^2/s) are used to define membrane and enzyme layer thicknesses and diffusion coefficients of the substrate in membrane and enzyme layer, respectively. The mass transfer coefficient on the feed side (m/s) was determined from an empirical correlation developed by Smith et al.[14].

$$\frac{k_s \times r}{D_{i,\infty}} = \alpha\, Re^{0.567} \times Sc^{0.33} \tag{7}$$

where r (m) defines the radius of the stirred cell, $D_{i,\infty}$, (m^2/s) is the free diffusivity of substrate, α is a dimensionless constant and definitions of Reynolds and Schmidt numbers are given below.

$$Re = \frac{\omega \times r^2}{v} \tag{8}$$

$$Sc = \frac{\mu_w}{\rho_w D_{i,\infty}} \tag{9}$$

where ω, (rev/s) is the stirring speed, v, (m^2/s), μ_w, (kg/m s) and ρ_w, (kg/m^3) are the kinematic viscosity, dynamic viscosity, and density of water, respectively. The free diffusivities of substrates were obtained from the empirical correlation of Wilke-Chang.

$$D_{i,\infty} = \frac{117.3 \times 10^{-18} (\phi M_w)^{1/2} T}{\mu_w v_A^{0.6}} \tag{10}$$

where, in this equation, ϕ, defines the association factor for water, and v_A, ($m^3/kmol$) is the molar volume of substrate. The resulting urea and BAPNA diffusivities in water at 25 °C were estimated as 1.48×10^{-5} and 3.85×10^{-6} cm^2/s respectively.

The mass transfer coefficient of substrate on the permeate side, k_p, (m/s), was calculated from the thickness of the boundary layer, δ_p, (m), and free solution diffusivity as follows;

$$k_p = \frac{D_{i,\infty}}{\delta_p} \tag{11}$$

The solute diffusivities (effective diffusivity, $D_{eff,i}$) in the enzyme layers and in the membrane were calculated by multiplying the free solution diffusion coefficients with the partition coefficient, Φ_i, porosity, ε, and diffusive hindrance factor, $K_{i,D}$.

$$D_{eff,i} = \varepsilon_i \Phi_i K_{i,D} D_{i,\infty} \tag{12}$$

The solute diffusive hindrance factor, $K_{i,D}$, is a function of the ratio between the solute and the pore diameters $(\lambda_i = d_{i,s}/d_p)$[15]. If parabolic fully developed solute flow within the pore is assumed, the diffusive hindrance factor can be defined as[16]:

$$K_{i,D} = 1.0 - 2.30\lambda_i + 1.154{\lambda_i}^2 + 0.224{\lambda_i}^3 \tag{13}$$

The partition coefficient in Equation (12) was calculated by assuming spherical solutes in cylindrical pores and the expression is given below.

$$\Phi_i = (1 - \lambda_i)^2 \tag{14}$$

In the case of TRY immobilized membrane, the substrate, BAPNA, first diffuses to the external surface of the membrane and then through the pores within the membrane where reaction takes place on the catalytic surface of the pores. The relative importance of the internal mass transfer over the rate of the reaction can be compared by the magnitude of Thiele modulus, κ, with the expression given below.

$$\kappa = \left(\frac{V_{\max}}{D_{eff,m} S_o}\right)^{\frac{1}{2}} L_{\text{mem}} \tag{15}$$

3. Results and discussion

3.1. Permeability studies

3.1.1. Buffer permeability

A preliminary experiment based on a protein analysis from permeate demonstrated that the AN69-PEI membrane completely rejects the urease so, surface immobilization without altering the membrane pores is

assumed. **Figure 3** shows the hydraulic permeabilities of buffer solutions normalized to the permeability in the plain AN69-PEI membrane. URE immobilization on this support slightly reduced the permeability (6%). The decrease might be attributed to the repulsion effect between mono and di-valent phosphate ions ($H_2PO_4^-$, HPO_4^{-2}) and the negatively charged groups available on the urease molecules. It is well known that species with the same charges as the membrane are more rejected than those with the opposite charges, increasing the formation of diffuse double layer and increasing the mass transfer resistance to buffer transport, resulting in a lower flux[17–19].

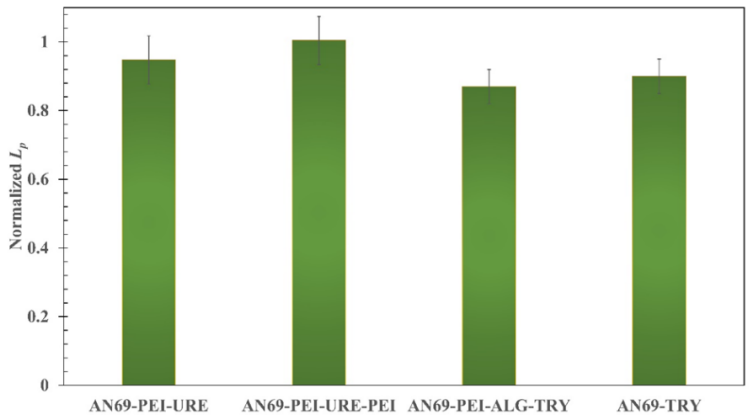

Figure 3. Normalized hydraulic permeabilities of buffer solution through URE and TRY immobilized membranes.

The normalized buffer permeabilities decreased by 13% and by 12% upon TRY immobilization on AN69 and AN69-PEI-ALG membranes due to penetration of the TRY into the pores and reduction in pore sizes as shown in our previous study with SEM pictures[10].

3.1.2. Substrate permeability

Figure 4 shows the influence of urea concentration on the normalized hydraulic permeabilities. Immobilizing URE between two polyelectrolytes (AN69-PEI-URE-PEI membrane) enhanced the urea permeabilities at all concentrations compared to the buffer permeability. Urea has a small dissociation constant in water and does not ionically interact with the membrane surface or its pores. Besides, it freely permeates through the membrane, with a pore diameter around 40 nm[10] due to its small molecular size (3.75 Å). Although urea and phosphate anions have similar sizes, the charged molecules' interactions in buffer solution with the membrane surface/pores resulted in lower buffer flux than urea[20].

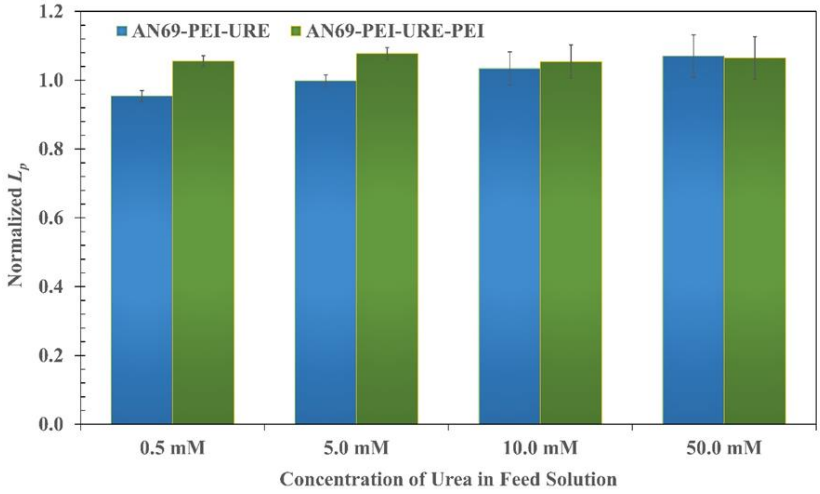

Figure 4. Normalized hydraulic permeabilities of urea solution through URE immobilized membranes.

The hydraulic permeabilities in the AN69-PEI-URE membrane increased with the increased urea concentration. Urease immobilized in this membrane directly contacts the feed solution, providing rapid reaction product, mainly ammonium cations (NH_4^+). As the reaction proceeds, the increase in NH_4^+ concentration may alter the enzyme and polyelectrolyte conformations via protonating or de-protonating. The attraction forces between mono/divalent phosphate ions and polyelectrolyte chains are reduced with the introduction of ammonium ion with mobilities higher than phosphate anions, causing a chain shielding; the chain may undergo a variation from the coil to extended conformation. When the AN69-PEI-URE membrane was used, the retentates' pH values were higher than the filtrated solution's pH. This observation demonstrated that some of the ammonium ions resulting from the biocatalytic reaction diffused back into feed solution. However, the ammonium's back-diffusion was restricted when URE was sandwiched between two polyelectrolyte layers (AN69-PEI-URE-PEI).

The influence of BAPNA concentration on the TRY immobilized membranes' hydraulic permeabilities is presented in **Figure 5**. The most prominent reduction in the permeability upon immobilization was observed for the AN69-PEI-ALG-TRY-ALG membrane. Sandwiching the TRY between ALG layers hinders the accessibility of BAPNA to the active site of TRY, hence decreases the activity of the membrane. The hydraulic permeability is influenced by the catalytic activity of TRY since the product of the catalytic reaction, p-NA, is much smaller than BAPNA and permeates faster compared to BAPNA in the solution. Another reason for the decrease in hydraulic permeability might be the charge repulsion between the functional groups in ALG and small species in the feed solution.

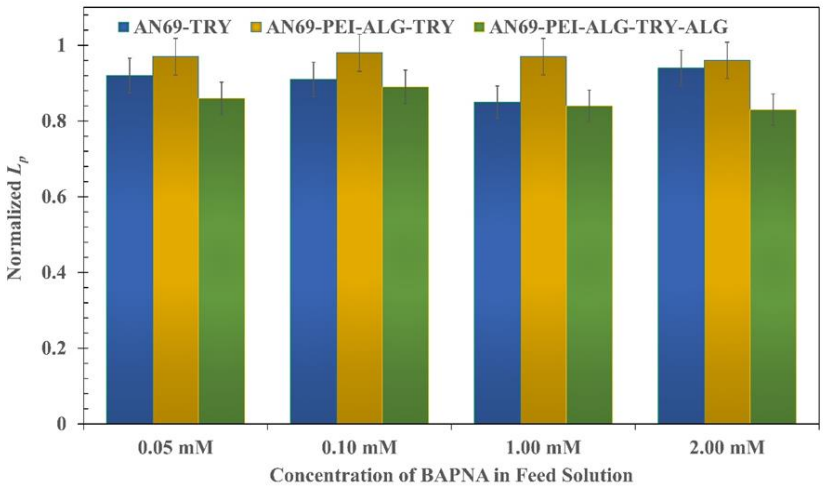

Figure 5. Normalized hydraulic permeabilities of BAPNA solution through TRY immobilized membranes.

3.2. Characterization of catalytic activity of the membranes

At the end of the filtration process, ammonia and p-NA concentrations in permeate and retentate sides formed through the catalytic decomposition of urea and BAPNA were determined. According to **Figure 6a**, ammonia formation increased with increasing its concentration in the feed solution up to urea concentration of 5 mM above which the catalytic membrane decomposed urea at the same rate. The result indicated that urea molecules occupied all URE catalytic active sides; hence, further increase in urea concentration did not cause any change in the conversion. At concentrations higher than 0.5 mM, increasing the volumetric flux shortened the urea molecules' residence time to contact URE; consequently, the ammonia formation rate decreased.

The p-NA formation in/on the AN69 membrane increased until one mM BAPNA concentration; then it started to decrease, as illustrated in **Figure 7a**. Considering the microenvironment inside the membrane, the local concentration of BAPNA is critical, entailing an inhibition effect and decrease in the enzymatic kinetics. At each BAPNA concentration, first, p-NA concentration increased with flux then reached a plateau. The result

demonstrated that the catalytic membrane works in a diffusion-controlled region; thus, TRY can degrade BAPNA into p-NA without affected by shorter residence time. In **Figure 7b**, a similar trend was observed for the AN69-PEI-ALG membrane. At concentrations higher than 0.1 mM, the p-NA formation decreased at high solution fluxes. Although the quantity of TRY adsorbed on AN69 and AN69-PEI-ALG membranes is almost equivalent (**Table 1**), the catalytic conversion on the AN69 was found lower. The result demonstrated that the ALG allows a more effective conformation of the TRY than that on the bare AN69 membrane.

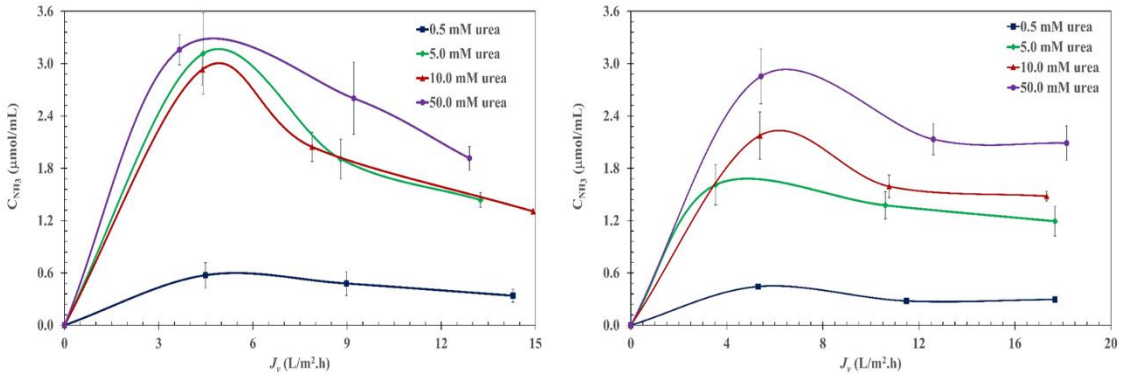

(a) **(b)**

Figure 6. Ammonia formation through catalytic decomposition of urea by **(a)** AN69-PEI-URE; and **(b)** AN69-PEI-URE-PEI membrane.

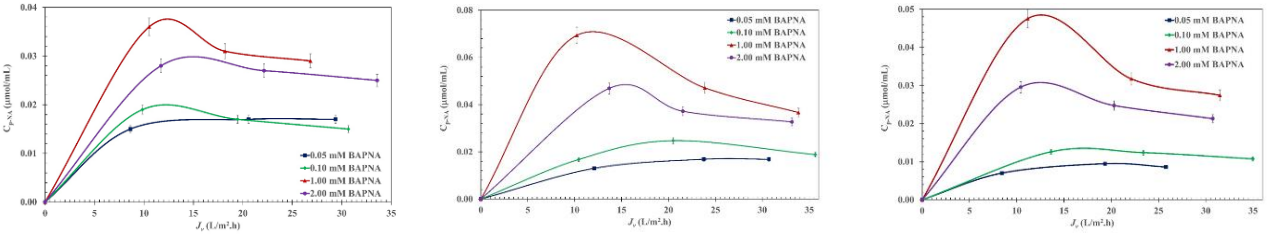

(a) **(b)** **(c)**

Figure 7. p-NA formation through catalytic decomposition of BAPNA by **(a)** AN69-TRY; **(b)** AN69-PEI-ALG-TRY; and **(c)** AN69-PEI-ALG-TRY-ALG membrane.

To increase the stability of enzyme molecules under pressure, they were sandwiched between the polyelectrolytes. As shown in **Figure 6b**, the AN69-PEI-URE-PEI's catalytic behavior differed from that of the AN69-PEI-URE membrane. The difference can be attributed to a change in the enzyme conformation, affecting the enzyme kinetic parameters. When URE was sandwiched between the PEI layers, the ammonia formation rate increased with the increased urea concentration from 0.5 to 50 mM, indicating that urease is not fully saturated even at the highest substrate concentration. Also, the rate did not decrease at high fluxes.

Sandwiching the TRY enzyme between two ALG layers did not enhance the catalytic activity (**Figure 7c**). The ALG cannot diffuse into pores due to its size larger than the pore size. Thus, most enzyme molecules immobilized in the pores are not protected with the ALG layer.

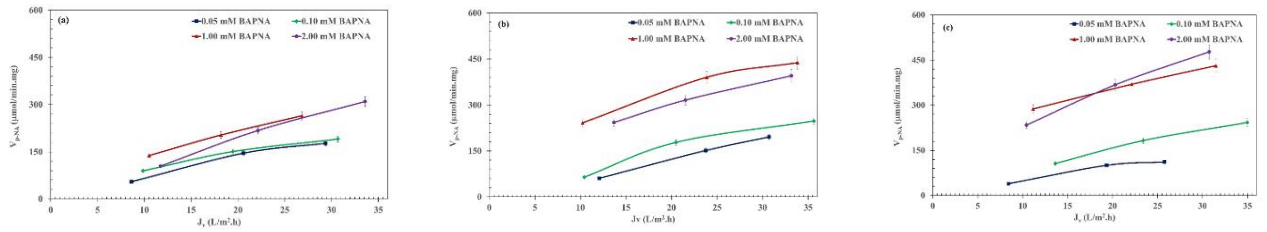

(a) **(b)** **(c)**

Figure 8. The variation of p-NA formation rate with respect to solution flux through **(a)** AN69-TRY; **(b)** AN69-PEI-ALG-TRY; and **(c)** AN69-PEI-ALG-TRY-ALG membranes.

The reaction rates of TRY immobilized membranes as a function of flux have been illustrated in **Figure 8**. The rates change linearly with respect to the flux. The reaction rates for the two types of URE immobilized membranes increased up to 0.85 bar, as shown in **Figure 9a,b**. The decrease in the rate above 0.85 bar could be attributed to the loss of enzyme or conformational change under high pressure.

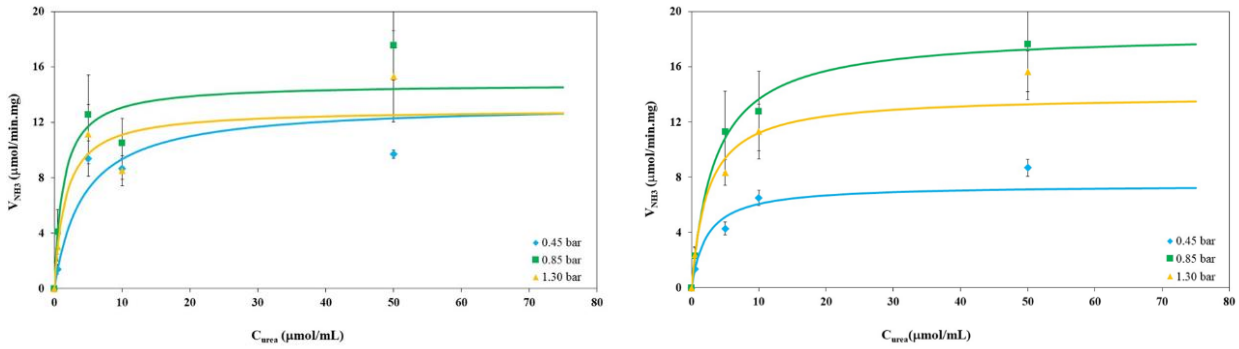

(a) **(b)**

Figure 9. Reaction rate of **(a)** AN69-PEI-URE; and **(b)** AN69-PEI-URE-PEI membrane as a function of substrate concentration. Points represent the experimental measurements and the lines are corresponding Michaelis-Menten fits.

Figure 10 demonstrates that all TRY architectures' reaction rates increased with increasing pressure. The highest activity was achieved when TRY was in sandwiched form, confirming the polyelectrolytes' positive effect on the enzyme conformation (**Figure 10c**).

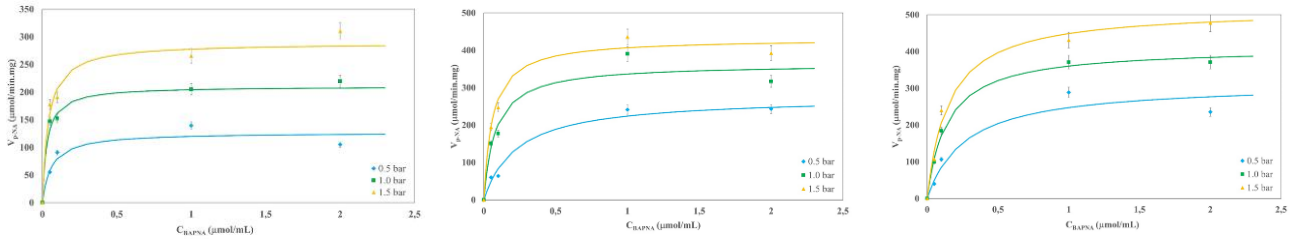

(a) **(b)** **(c)**

Figure 10. Reaction rate of **(a)** AN69-TRY; **(b)** AN69-PEI-ALG-TRY; and **(c)** AN69-PEI-ALG-TRY-ALG membrane as a function of substrate concentration.
Points represent the experimental measurements and the lines are corresponding Michaelis-Menten fits.

The kinetic parameters of the membranes, V_{max} and K_m, and turnover number, k_{cat}, as a function of transmembrane pressure are summarized in **Table 2**. The AN69-PEI-URE exhibited higher activity at static conditions ($\Delta P = 0$) than its activities measured under dynamic conditions. Since URE in this architecture is directly contacted with the feed solution, the pressure's conformational change would be inevitable. In contrast, when URE was in the sandwiched form, the membrane's activity increased with the pressure. The sandwiched architecture serves a better microenvironment for conformational stability. The convective force is then utilized to compensate/eliminate the mass transfer resistance due to additional layer and product inhibition due to back diffusion. TRY, which was immobilized primarily in the membrane pores, had lower activities under pressure than the static condition. This result can be explained by the significant difference between the pore size of the membrane (40 nm) and the size of TRY molecules (4.8 nm × 3.7 nm × 3.2 nm)[21], resulting in the conformational change under pressure. Chen et al. investigated the influence of membrane pore diameter on the lipase activity immobilized in the PSF MF hollow fiber membrane[22]. They observed the highest activity with the largest pore-sized membrane at low transmembrane pressure while at high transmembrane pressure, with the smallest pore size. This observation supports our hypothesis that the enzyme in the large pores is more susceptible to conformational change at high pressures. The increase in TRY immobilized membranes'

catalytic activity with pressure can be attributed to the shorter residence time and more negligible product inhibition effect. The highest activity has been attained when TRY was in the sandwiched form which, demonstrated the beneficial effect of polyelectrolytes on protecting the enzyme conformation. Not only the k_{cat} value but also the k_{cat}/K_m ratio determines the catalytic efficiency of an enzyme. Compared to the static conditions, the decrease in the k_{cat}/K_m values for the TRY under dynamic conditions implied that its immobilization platform is not suitable.

Table 2. Kinetic parameters of the URE and TRY immobilized membranes.

	ΔP	V_{max}	K_m	k_{cat}	$k_{cat}/K_m \times 10^{-3}$
Membrane	**(bar)**	**(μmol/min mg)**	**(μmol/mL)**	**(min^{-1})**	**(min^{-1}/mM^{-1})**
Free urease	0.00	949.5	10.4	1.7×10^8	16,859
AN69-PEI-URE	0.00	23.8	10.6	12,800	1.2
	0.45	13.3	4.27	7248	1.7
	0.85	14.8	1.31	8066	6.2
	1.30	13.0	1.65	7085	4.3
AN69-PEI-URE-PEI	0.00	5.4	2.00	3200	1.6
	0.45	7.5	2.26	4087	1.8
	0.85	18.5	3.50	10,082	2.9
	1.28	13.9	2.42	7575	3.1
Free trypsin	0.00	1.8×10^6	0.95	4.4×10^7	4.6×10^4
AN69-TRY	0.00	7980	0.24	3.4×10^5	1416.7
	0.50	127.1	0.06	3025	50.4
	1.00	210.5	0.03	5010	167.0
	1.50	288.9	0.04	6876	171.9
AN69-PEI-ALG-TRY	0.00	11,830	0.47	5.4×10^5	1148.9
	0.50	275.8	0.23	6564	28.5
	1.00	363.6	0.08	8654	108.2
	1.50	431.1	0.06	10,260	171.0
AN69-PEI-ALG-TRY-ALG	0.00	9610	0.57	3.3×10^5	578.9
	0.50	314.3	0.27	7480	27.7
	1.00	410.8	0.14	9777	69.8
	1.50	516.1	0.15	12,283	81.9

In enzymatic membrane bioreactors, mass transfer and reaction processes occur simultaneously. Damköhler number and Thiele modulus were calculated to determine the controlling step for the catalytic degradation of urea and BAPNA. Except for the lowest urea concentration, Damköhler numbers at other concentrations and all pressures were found less than one (**Table 3**). These values demonstrated urea degradation occurs in the reaction-limited region. At the same urea concentration and transmembrane pressure, Da was higher for the AN69-PEI-URE-PEI than for the AN69-PEI-URE indicating higher mass transfer resistance in the sandwich configuration.

TRY immobilized membranes degraded BAPNA in the mass transfer-limited regime as confirmed by the Thiele modulus values close to 1 or greater than 1 (**Table 3**). Another indication of mass transfer limitation for the catalytic degradation of BAPNA is the linear increase in TRY activity with the solution flux, as shown in **Figure 8**. According to **Table 4**, the highest diffusional limitation occurred when TRY was sandwiched between ALG layers. The highest k_{cat} value determined for the AN69-PEI-ALG-TRY-ALG (**Table 2**) indicated

the benefit of diffusional limitation in enhancing the degradation of BAPNA. The mass transfer resistance decreased with the increased BAPNA concentration, but the reaction still took place in the mass transfer-limited regime since BAPNA should first traverse the external film and diffuse through the membrane to reach the TRY's active sides. The external mass transfer resistance is easily eliminated by allowing a higher stirring rate for the substrate solution. On the other hand, internal mass transfer resistance can be eliminated by changing the membrane's structural properties, such as its thickness, pore size, porosity, and tortuosity.

Table 3. The change in Damköhler number with respect to urea concentration at three different pressures for the URE immobilized membranes.

Membrane		**Δ*P* (bar)**		
	C_{urea} (mM)	**0.45**	**0.85**	**1.30**
AN69-PEI-URE	0.5	7.51	9.54	8.82
	5.0	0.75	0.95	0.88
	10.0	0.38	0.48	0.44
	50.0	0.08	0.10	0.09
AN69-PEI-URE-PEI	0.5	8.26	10.29	11.45
	5.0	0.83	1.03	1.15
	10.0	0.41	0.51	0.57
	50.0	0.08	0.10	0.11

Table 4. The change in Thiele modulus with respect to BAPNA concentration at three different pressures for the TRY immobilized membranes.

Membrane		**Δ*P* (bar)**		
	C_{BAPNA} (mM)	**0.5**	**1.0**	**1.5**
AN69-TRY	0.05	6.91	7.63	8.73
	0.10	4.89	5.40	6.18
	1.00	1.55	1.71	1.95
	2.00	1.09	1.21	1.38
AN69-PEI-ALG-TRY	0.05	7.56	10.63	11.68
	0.10	5.34	7.52	8.26
	1.00	1.69	2.38	2.61
	2.00	1.19	1.68	1.85
AN69-PEI-ALG-TRY-ALG	0.05	16.80	10.07	11.92
	0.10	11.88	7.12	8.43
	1.00	3.76	2.25	2.67
	2.00	2.66	1.59	1.89

The stabilities of enzyme activities were tested by measuring membranes' catalytic activities at the end of 450 min of filtration. According to the results shown in **Figure 11**, the AN69-PEI-URE-PEI and AN69-PEI-URE membranes lost 8% and 50% of their initial activities. The activity loss of all TRY immobilized membranes was found similar. The results demonstrated that the URE in the sandwiched form maintained most of its initial activity in the long-term filtration. In contrast, different LbL architectures did not help in improving the activity loss of TRY under pressure.

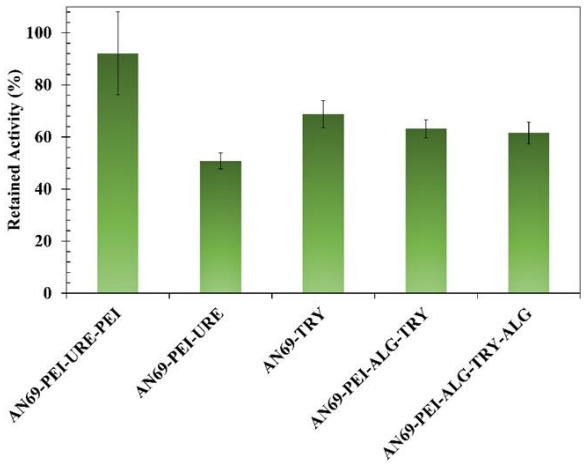

Figure 11. The retained activity of the catalytic membranes (%) at the end of 450 min of filtration process.

4. Conclusion

In this study, we studied the effects of enzyme location on the catalytic activity, long-term stability, and mass transfer resistance of the AN69 membranes. The filtration and catalytic performances of the prepared membranes were determined under dynamic conditions. Compared to the buffer permeability, urea solutions' hydraulic permeabilities in various concentrations across the URE immobilized membranes did not change significantly. Indeed, an enhanced permeability was observed at high urea concentrations. The permeability of the TRY immobilized membranes did not vary with the concentration of the substrate solution. However, TRY immobilization decreased the permeability due to its attachment to membrane pores.

The reaction rates increased with increasing transmembrane pressures for the TRY immobilized membranes, but the maximum rate was achieved at 1 bar in the case of URE immobilized membranes. The experimental data and calculated dimensionless numbers indicated that the degradation of urea occurs in the reaction-limited region; on the contrary, the mass transfer is the rate-controlling step for converting BAPNA. The highest catalytic activities for the URE and TRY immobilized membranes were observed when they were both immobilized in sandwiched form between two polyelectrolytes. This configuration prevented conformational variation of URE and product back-diffusion during filtration, hence provided long-term stability. On the other hand, LbL architectures could not prevent the TRY activity loss in the long term under pressure. The results suggested that when the enzyme is mostly immobilized in the pores, the polyelectrolytes' molecular weight should be smaller than the MWCO of the membrane. In this case, the LbL assembly will protect enzymes not only on the surface but also in the membrane's pores.

Author contributions

Conceptualization, YY and CI; methodology, YY and SG; formal analysis, YY and SG; writing—original draft preparation, YY and SG; writing—review and editing, SAA, AD and CI; visualization, YY and CI; supervision, SAA and AD; project administration, SAA and AD. All authors have read and agreed to the published version of the manuscript.

Acknowledgments

The authors would like to thank the Ministry of Foreign Affairs of the Republic of France and the Scientific and Technical Research Council of Turkey (Grant Number: 105M325) for partial funding (IFC), the Gambro-Hospal, Lyon, France for kindly providing the AN69 and AN69-PEI membranes.

Conflict of interest

The authors declare no conflict of interest.

References

1. Inamdar STA. *Biochemical Engineering: Principles and Concepts*, 3rd ed. PHI; 2012.
2. Rodrigues RC, Ortiz C, Berenguer-Murcia Á, et al. Modifying enzyme activity and selectivity by immobilization. *Chemical Society Reviews* 2013; 42(15): 6290–6307. doi: 10.1039/c2cs35231a
3. Bayne L, Ulijn RV, Halling PJ. Eff ect of pore size on the performance of immobilised enzymes. *Chemical Society Reviews* 2013; 42(23): 9000. doi: 10.1039/c3cs60270b
4. Liu Y, Lu H, Zhong W, et al. Multilayer-assembled microchip for enzyme ımmobilization as reactor toward low-level protein ıdentification. *Analytical Chemistry* 2005; 78(3): 801–808. doi: 10.1021/ac051463w
5. Yong JKJ, Cui J, Cho KL, et al. Surface engineering of polypropylene membranes with carbonic anhydrase-loaded mesoporous silica nanoparticles for ımproved carbon dioxide hydration. *Langmuir* 2015; 31(22): 6211−6219. doi: 10.1021/acs.langmuir.5b01020
6. Dizge N, Epsztein R, Cheng W, et al. Biocatalytic and salt selective multilayer polyelectrolyte nanofiltration membrane. *Journal of Membrane Science* 2018; 549: 357–365. doi: 10.1016/j.memsci.2017.12.026
7. Datta S, Cecil C, Bhattacharyya D. Functionalized membranes by layer-by-layer assembly of polyelectrolytes and ın situ polymerization of acrylic acid for applications in enzymatic catalysis. *Industrial & Engineering Chemistry Research* 2008; 47(14): 4586–4597. doi: 10.1021/ie800142d
8. Sarma R, Islam MdS, Miller AF, Bhattacharyya D. Layer-by-layer-assembled laccase enzyme on stimuli-responsive membranes for chloro-organics degradation. *ACS Applied Materials & Interfaces* 2017; 9(17): 14858−14867. doi: 10.1021/acsami.7b01999
9. Dong J, Ning W, Liu W, Bruening ML. Limited proteolysis in porous membrane reactors containing ımmobilized trypsin. *Analyst* 2017; 142(14): 2578–2586. doi: 10.1039/c7an00778g
10. Guedidi S, Yurekli Y, Deratani A, et al. Effect of enzyme location on activity and stability of trypsin and urease immobilized on porous membranes by using layer-by-layer self-assembly of polyelectrolyte. *Journal of Membrane Science* 2010; 365(1–2): 59–67. doi: 10.1016/j.memsci.2010.08.042
11. Yurekli Y, Alsoy SA. Catalytic performances of chemically immobilized urease under static and dynamic conditions: A comparative study. *Journal of Molecular Catalysis B: Enzymatic* 2011; 71(1–2): 36–44. doi: 10.1016/j.molcatb.2011.03.006
12. Langsdorf LJ, Zydney AL. Diffusive and convective transport through hemodialysis membranes: Comparison with hydrodynamic predictions. *Journal of Biomedical Materials Research* 1994; 28: 573–582. doi: 10.1002/jbm.820280507
13. Bradford MM. A rapid and sensitive method for the quantitation of microgram quantities of protein utilizing the principle of protein-dye binding. *Analytical Biochemistry* 1976; 72: 248–254. doi: 10.1006/abio.1976.9999
14. Smith KA, Colton CK, Merril EW, Evans LB. The artificial Kidney; *Chemical Engineering Progress Symposium Series* 1968; 64: 45.
15. Deen WM. Hindered transport of large molecules in liquid ‐ filled pores. *AIChE Journal* 1987; 33(9): 1409–1425. doi: 10.1002/aic.690330902
16. Bowen WR, Mohammad AW, Hilal N. Characterisation of nanofiltration membranes for predictive purposes—use of salts, uncharged solutes and atomic force microscopy. *Journal of Membrane Science* 1997; 126(1): 91–105. doi: 10.1016/S0376-7388(96)00276-1
17. Mika AM, Childs RF, Dickson JM, et al. A new class of polyelectrolyte-filled microfiltration membranes with environmentally controlled porosity. *Journal of Membrane Science* 1995; 108(1–2): 37–56. doi: 10.1016/0376-7388(95)00140-2
18. Marshall AD, Munro PA, Trägardh G. The effect of protein fouling in microfiltration and ultrafiltration on permeate flux, protein retention and selectivity: A literature review. *Desalination* 1993; 91(1): 65–108. doi: 10.1016/0011-9164(93)80047-Q
19. Musale DA, Kulkarni SS. Effect of membrane-solute interactions on ultrafiltration performance. *Journal of Macromolecular Science, Part C: Polymer Reviews* 1998; 38(4): 615–636. doi: 10.1080/15583729808546034
20. Naitou A, Oinuma M, Ozawa K, et al. Effects of charge density on electrolyte transport through dialysis membranes. *Japanese Society for Artificial Organs* 1987; 16(2): 703–706. doi: 10.11392/jsao1972.16.703
21. Koutsopoulos S, Patzsch K, Bosker WTE, Norde W. Adsorption of trypsin on hydrophilic and hydrophobic surfaces. *Langmuir* 2007; 23(4): 2000–2006. doi: 10.1021/la062238s
22. Chen PC, Ma Z, Zhu XY, et al. Fabrication and optimization of a lipase ımmobilized enzymatic membrane bioreactor based on polysulfone gradient-pore hollow fiber membrane. *Catalysts* 2019; 9(6): 495. doi: 10.3390/catal9060495